A Unified Field Analysis Method for IR/MMW Beam Splitter

Yi Tian[1,2,3], **Hui Yan**[1,3], **Xin Wang**[1,3], **Li Zhang**[2], **and Zhuo Li**[1,3]

[1]School of Opto-Electronics, Beijing Institute of Technology, Beijing 100081, China
[2]Shanghai Institute of Electro-Mechanical Engineering, Shanghai 201109, China
[3]Beijing Key Lab for Precision Optoelectronic Measurement Instrument and Technology
Beijing 100081, China

Abstract— Aperture field integration method (AFIM) is proposed and utilized to efficiently compute the field distributions of infrared (IR)/millimeter wave (MMW) beam splitter including the MMW near field distribution and IR far field distribution. A single dielectric layer beam splitter is analyzed by AFIM. Compared to the multilevel fast multipole method (MLFMM), the memory requirement and CPU time consumption are reduced drastically from 4.6 GB and 2141 seconds to 1.2 MB and 58 seconds, respectively, when the MMW near field distribution is computed. In order to meet the far field condition a scale factor is proposed to transform the focal plane into a far field plane, when the IR far field in a focal plane is computed. The IR far field calculation accuracy is better than 97% compared to the analytical solutions. The simulation results show that the AFIM as a unified method can be applied to both beam splitters' MMW near field and IR far field engineering estimation.

1. INTRODUCTION

An IR/MMW dual-mode compound guidance system has both high-precision infrared imaging and all-weather-working millimeter wave imaging advantages at the same time. IR/MMW beam splitter is a key component of dual-mode compound guidance system. The beam splitter is tilted by 45° along the main axis and it transmits MMW signals and reflects IR signals at the same time as shown in Fig. 1. Its role is to spatially split the IR and MMW compound signal into a reflected IR signal received by an IR sensor in the vertical direction and a transmitted MMW signal received by a MMW sensor in the horizontal direction respectively [1].

Many types of beam splitters have been proposed, such as dielectric coated with an array of small conducting patches [2], holographic optical elements [3], frequency selective surface [4], conducting inductive meshes with periodic rectangle units [1] micro-mirror array [5], multilayered dielectric plate [6] and so forth.

No matter which kind of beam splitter is inserted in the dual-mode compound guidance system, the insertion of a beam splitter will affect the uniformity of the MMW field. Simultaneously, the insertion also affects the IR imaging quality. Moreover, the detecting and tracking precision will be limited by the distortion of the filed received by MMW and IR sensors [5–7]. Therefore, it is necessary to build a theoretical model to analyze the MMW and IR field distribution. Generally, the calculation of electrical field in a MMW sensor aperture is a near field diffraction problem. However the calculation of optical field focused on an IR focal plane array through an IR lens is a far field diffraction problem. Nevertheless, both IR and MMW are electromagnetic wave and they can be described by Maxwell-Equations. So the MMW near field and IR far field problem can be solved by a unified method derived from integral formulation of Maxwell-Equations. Thus,

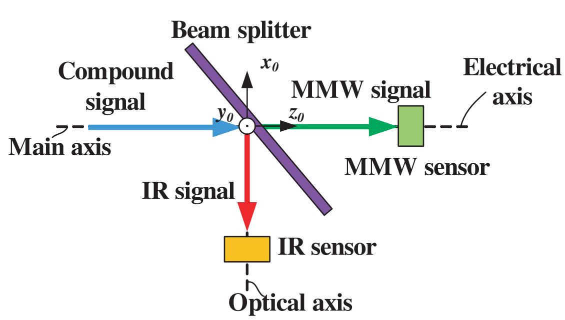

Figure 1: Working principle of beam splitter.

aperture field integration method (AFIM) is proposed to analyze both MMW near field and IR far field of beam splitters in this paper.

In Section 2 the basic theory and formulations about AFIM are introduced. In Section 3, the method is investigated through the calculation of a circular single layer beam splitter. The calculation results of MMW field are described and compared with MLFMM. The calculation results of IR field are also described and compared with the analytical solution. In the last section a brief conclusion is made.

2. METHODS AND FORMULATIONS

In order to obtain the diffracted field, the beam splitter is simplified to a 2D aperture as shown in Fig. 2. According to the equivalence principle, the field produced by the beam splitter current could be obtained by computing the field of the aperture equivalent source [8, 9]. In this way, the analysis of the beam splitter can be converted to the analysis of the aperture.

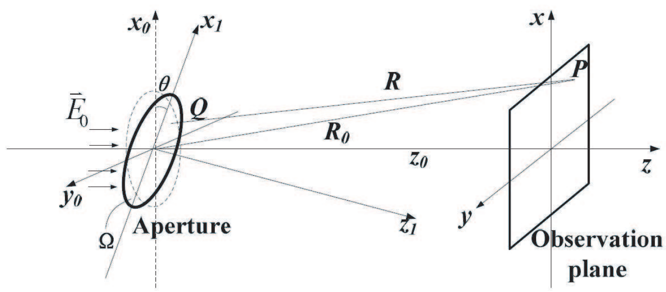

Figure 2: Principle of AFIM.

Assume that the aperture is tilted by an angle of θ along the main axis as shown in Fig. 2. The incident wave can be assumed as plane wave. The aperture field can be expressed as [1]

$$\vec{E}_A(x_1, y_0) = \vec{E}_0 \exp[-j(k_0 x_0 \tan\theta)] \tag{1}$$

where, k_0 is the wave number, $\vec{E}_0$ is the amplitude vector of polarized electrical field. According to the equivalence principle, the equivalent magnetic current is expressed as [9]

$$\vec{J}_m = -\hat{z} \times \vec{E}_A \tag{2}$$

The electrical vector potential is

$$\vec{A}_m = \frac{\varepsilon}{4\pi} \iint_\Omega \frac{\vec{J}_m e^{-jk_0 R}}{R} \mathrm{d}x_1 \mathrm{d}y_0 \tag{3}$$

The field at an arbitrary observation point P is [9]

$$\vec{E}(x, y) = -\frac{1}{\varepsilon} \nabla \times \vec{A}_m = -\frac{1}{4\pi} \iint_\Omega \left[R \times \left(\hat{z} \times \vec{E}_A\right)\right] \cdot (1 + jk_0 R) \frac{e^{-jk_0 R}}{R^3} \mathrm{d}x_1 \mathrm{d}y_0 \tag{4}$$

where R is the distance between the source point Q and field point P, which can be expressed as [1]

$$R = \sqrt{(x - x_0)^2 + (y - y_0)^2 + (z_0 - x_0 \tan\theta)^2} \tag{5}$$

where, z_0 is the distance between the aperture and the observation plane. The integration is over the aperture region Ω.

The near field and far field can be obtained by computing the Eq. (4). However, the far field distribution in a focal plane can't be obtained by directly solving the Eq. (4) because of the phase transformation by a lens with focal length of f. In order to calculate the far field distribution in a focal plane, a scale factor η is introduced to transform the focal plane to a far field plane. η should meet the far field condition [10]:

$$\eta \le \frac{2r^2}{\lambda f} \tag{6}$$

where, r is the circumcircle radius of the aperture region Ω.

So the far field in a focal plane can be expressed as

$$\vec{E}_{far}(x',y') = -\frac{1}{4\pi}\iint_{\Omega}\left[R'\times\left(\hat{z}\times\vec{E}_A\right)\right]\cdot\left(1+jk_0R'\right)\frac{e^{-jk_0R'}}{R'^3}\mathrm{d}x_1\mathrm{d}y_0 \tag{7}$$

where, $R' = \eta f$, $x' = \eta x$, $y' = \eta y$.

3. NUMERICAL EXAMPLE AND VALIDATION

3.1. Beam Splitter Example

In order to validate our computation method, a single layer circular beam splitter with IR film is analyzed. It is made of lossless material with relative dielectric constant of 3.8. Its thickness is 2 mm. The radius r of the beam splitter is 50 mm. The surface is coated with IR film proposed in [6]. The beam splitter is 45° tilted angles placed relative to the electrical axis of the MMW sensor. The distance between the MMW sensor and the beam splitter is 50 mm. It is designed for the MMW with 35 GHz frequency. The observation plane of the MMW sensor is assumed to be a square region with an edge length of 70 mm. The working center wavelength of IR is 4 μm. The focal length of IR sensor objective lens is 120 mm. The observation plane of the IR sensor is assumed to be a square region with an edge length of 100 μm.

3.2. MMW Near Field Validation

In order to validate the MMW near field computation ability of AFIM, the calculation results are compared with the results obtained by MLFMM, because MLFMM is considered to be a high precision computation [5, 7]. The computations made by AFIM and MLFMM are carried out on the same computer equipped with two 2.50 GHz Intel® Xeon® CPUs (12 cores) and 128 GB memories. Both of the MLFMM and AFIM codes support parallel computation.

In both of the computations the observation plane is discretized equally to 81 divisions along x-axis and y-axis. In MLFMM computation the edge of the triangle mesh is $\lambda/8$. So the mesh number and mesh edges are up to 43232 and 64848, respectively. As comparison, the edge of the mesh is $\lambda/22$ in AFIM computation, which brought to a mesh number of 65536. The computational efficiency comparison with two methods is shown in Table 1. MLFMM consumes 4.6 GB memories and more than 30 minutes. However, AFIM uses only several MB memories and less than 1 minute, even though the mesh size in AFIM is less than that in MLFMM. The comparison indicates that AFIM is much more efficient than MLFMM.

Table 1: Comparison of computational efficiency.

Method	Mesh size	Unknown field point	Memory	Time
MLFMM	$\lambda/8$	81×81	4.6 GB	2141s
AFIM	$\lambda/22$	81×81	1.2 MB	58s

In order to comparison, the amplitude and phase in observation plane are normalized by the value at ($x = 0$ mm, $y = 0$ mm). Figs. 3(a) and (b) are the amplitude distribution of MMW near field computed by AFIM and MLFMM, respectively. The maximum and minimum amplitudes computed by AFIM are 4.06 dB and −14.68 dB respectively as shown in Fig. 3(a). The maximum and minimum amplitudes computed by MLFMM are 2.94 dB and −12.56 dB respectively as shown in Fig. 3(b). However, the distributions of the amplitude obtained by the two methods match well. The maximum and minimum phases computed by AFIM are 43.68° and −61.87° as shown in Fig. 4(a). The maximum and minimum phases computed by MLFMM are 29° and −98.5° as shown in Fig. 4(b). Similarly, the patterns of the phase obtained by the two methods also match well. Compared with MLFMM, errors are introduced. One of reasons is that the beam splitter is equivalent to an aperture, and the detailed structure of the beam splitter is not considered in AFIM. However, compared to the commonly used MLFMM the memory requirement and CPU time consumption are reduced drastically. So AFIM can be used as an efficiency engineering approximation method.

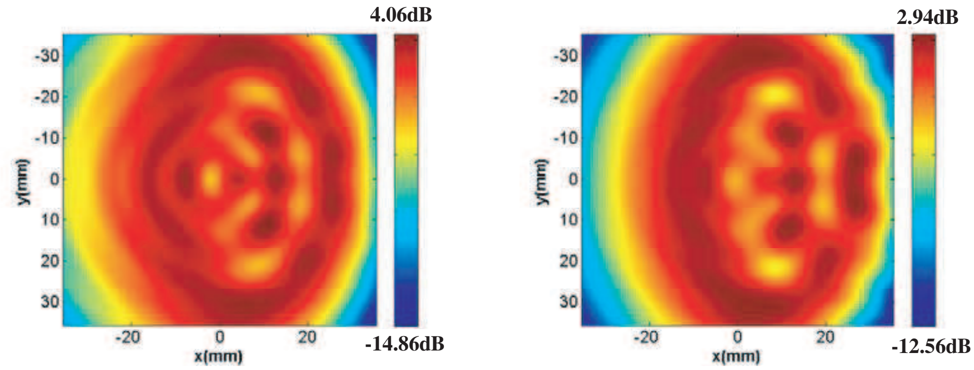

(a) (b)

Figure 3: Amplitude distribution of MMW near field in observation plane computed by (a) AFIM; (b) MLFMM.

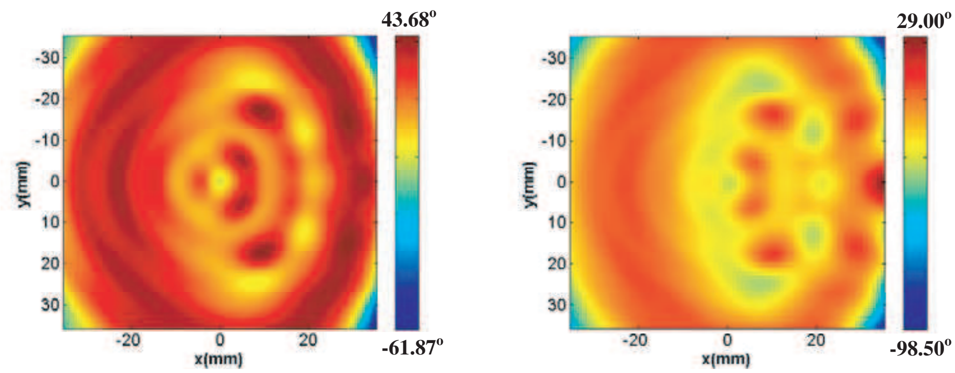

(a) (b)

Figure 4: Phase distribution of MMW near field in observation plane computed by (a) AFIM; (b) MLFMM.

3.3. IR Far Field Validation

In order to validate the computation ability of IR far field by using AFIM, the calculation results are compared with the results obtained by analytical solution [10]. The analytical solution (AS) can be expressed as

$$\vec{E}_{far}(x, y) = Cr^2 \cos\theta \frac{2J_1(\alpha)}{\alpha} \tag{8}$$

where α, C can be expressed as

$$\alpha = \frac{2\pi r\sqrt{(\beta_1 \cos\theta)^2 + y^2}}{\lambda R_0} \tag{9}$$

$$C = \frac{\vec{E}_0}{4\pi} \frac{jk_0 e^{-jk_0 R_0}}{R_0} \tag{10}$$

where, β_1 and R_0 can be expressed as

$$\beta_1 = x + \tan\theta\sqrt{R_0^2 - x^2 - y^2} - R_0 \tan\theta \tag{11}$$

$$R_0 = \sqrt{x^2 + y^2 + z_0^2} \tag{12}$$

The focal plane is a square region with edge length of 100 µm. It is 512 × 512 meshed. The aperture is 128 × 128 meshed for AFIM. In order to meet the far field condition, η should be larger than 1×10^4, and let $\eta = 1 \times 10^6$ in this paper. In order to quantitatively compare the results, the relative error of far field intensity I_{AFIM} computed by AFIM is calculated according to [11]

$$\frac{\|I_{AFIM} - I_{AS}\|}{\|I_{AS}\|} \tag{13}$$

where $\| \ \|$ is the 2-norm and I_{AS} is the reference solution computed by AS with mesh number of 512×512.

The normalized intensities of the IR far field computed by AFIM and AS are compared in Fig. 5. The error is only 0.14% as shown in Table 2. The relationship between the error, consumed time and mesh number of aperture is also listed in Table 2. The CPU time decreases drastically with the decrease of the mesh number. And the error increases with the decrease of mesh number. The right results can't be obtained when the mesh number of aperture is 8×8. To keep an error lower than 3%, the mesh number more than 16×16 is required by AFIM.

Table 2: Error and CPU time versus mesh number of aperture.

Mesh number	Error	CPU time
128×128	0.14%	612.00 s
64×64	0.51%	162.08 s
32×32	1.35%	74.44 s
16×16	2.30%	21.56 s
8×8	288.92%	8.34 s

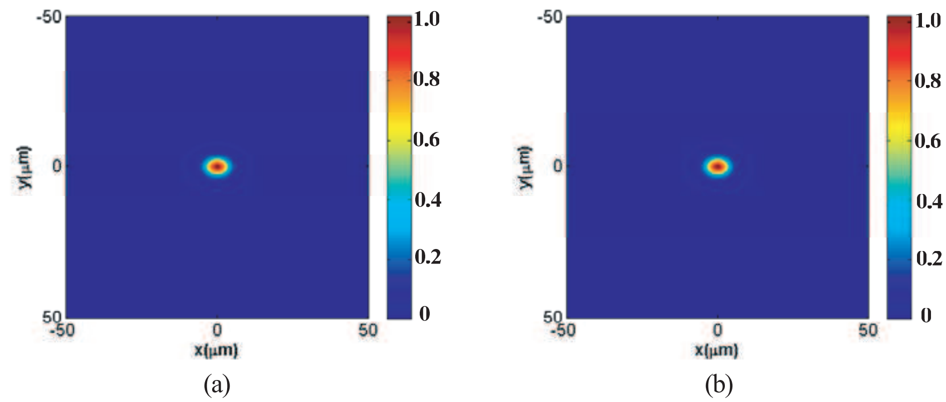

Figure 5: Normalized intensity distribution at focal plane computed by (a) AFIM; (b) AS.

The zero-order diffraction primary maximum widths along x-axis and y-axis acquired by AFIM are 16.56 μm and 11.86 μm, respectively. If $\theta = 0°$, the zero-order diffraction primary maximum diameter can be computed by $0.61\lambda f/r = 11.71$ μm. The simulation results show that the zero-order diffraction primary maximum width is stretched along x-axis while it remains unchanged along y-axis. The tilted angle will lead to increase the diffraction limit. Thus the resolution of the IR sensor will be decreased. It must be noted that the AFIM can also be used to analyze beam splitters with complex aperture shapes without analytical solution of far field.

4. CONCLUSIONS

According to equivalent principle, a unified method AFIM is proposed to compute field distribution of IR/MMW beam splitter including the MMW near field distribution and IR far field distribution For a single layer beam combiner, the patterns of the MMW amplitude and phase obtained by the MLFMM and AFIM match well. An appreciable speedup on the order of 40 is achieved. In order to meet the far field condition, the scale factor is proposed and it should be larger than 1×10^4 in the numerical example. The calculation accuracy is better than 97% for IR far field computation when the mesh number of the equivalent aperture is more than 16×16. The simulation results show that the AFIM can be used as an efficiency engineering approximation method in the design, analysis, and optimization of beam splitter.

REFERENCES

1. Liu, Y., J. Tan, and J. Ma, "Use of conducting inductive meshes with periodic rectangle units as an infrared/microwave dual-mode detecting beamsplitter," *J. Opt.*, Vol. 13, 035407, 6pp, 2011.
2. Mobley, S., J. Cole, J. Cooper, and J. Jarem, "U.S. Army Missile Command dual-mode millimeter wave/infrared simulator development," *Proc. SPIE*, Vol. 2741, 316–331, 1996.
3. Mobley, S. B. and J. Gareri, "Hardware-in-the-loop simulation (HWIL) facility for development, test, and evaluation of multi-spectral missile systems — Update," *Proc. SPIE*, Vol. 4027, 11–21, 2000.
4. Mobley, S. and J. Cole, "Dichroic beam combiner to support hardware-in-the-loop testing of dual-mode common aperture seekers," *Proc. SPIE*, Vol. 3368, 32–41, 1998.
5. Tian, Y., L. J. Lv, L. W. Jiang, X. Wang, Y. H. Li, H. M. Yu, X. C. Feng, Q. Li, L. Zhang, and Z. Li, "Infrared/microwave (IR/MW) micromirror array beam combiner design and analysis," *Appl. Opt.*, Vol. 52, 5411–5419, 2013.
6. Tian, Y., R. Xu, Rui. Shi, X. Wang, Q. Li, L. Zhang, and Z. Li, "IR/MW multilayered dielectric plate beam combiner design, optimization and evaluation," *Appl. Optics*, Vol. 52, 288–297, 2013.
7. Mobley, S., J. Cole, J. Cooper, and J. Jarem, "U.S. Army Missile Command dual-mode millimeter wave/infrared simulator development," *Proc. SPIE*, Vol. 2741, 316–331, 1996.
8. McKay, J. P. and R. S. Yahya, "Compact range reflector analysis using the plane wave spectrum approach with an adjustable sampling rate," *IEEE Trans. Antenna. Propag.*, Vol. 39, 746–753, 1991.
9. Quan, S., "Time domain analysis of the near-field radiation of shaped electrically large apertures," *IEEE Trans. Antenna. Propag.*, Vol. 58, 300–306, 2010.
10. Tan, J., Z. Lu, J. Liu, P. Jin, and Y. Wang, "Analysis of fraunhofer diffractive characteristics of a tilted metallic mesh for its effect on optical measurement," *Measurement Science and Technology*, Vol. 18, No. 6, 1703–1709, 2007.
11. Su, T., D. Ding, Z. Fan, and R. Chen, "Efficient analysis of EM scattering from bodies of revolution via the ACA," *IEEE Trans. Antenna. Propag.*, Vol. 62, No. 2, 983–985, Feb. 2014.